Heterogeneity of Functional Synaptic Parameters among Single Release Sites

Céline Auger, Alain Marty

Heterogeneity of Functional Synaptic Parameters among Single Release Sites

Céline Auger and Alain Marty
Arbeitsgruppe Zelluläre Neurobiologie, Max-Planck-Institut für biophysikalische Chemie, 37077 Göttingen, Federal Republic of Germany

Abstract

Following α-latrotoxin application to cerebellar slices, bursts of miniature IPSCs (mIPSCs) were observed in interneurons of the molecular layer. Within bursts, mIPSCs had homogeneous amplitudes with a narrow Gaussian distribution. Analysis of successive event amplitudes revealed an interaction between consecutive IPSCs, indicating that bursts originate at single release sites. A mean receptor occupancy of 76% was calculated. IPSCs within a burst were analyzed using nonstationary noise analysis. The results indicate that individual release sites differ in the number, unitary conductance, and peak opening probability of their postsynaptic channels. In addition, the IPSC decay kinetics were very different among release sites. Finally, a significant correlation was found between several pairs of single site synaptic parameters.

Introduction

A major difficulty for quantitative studies of synaptic transmission in the central nervous system stems from the fact that postsynaptic signals usually originate from several release sites. As a result, it has been difficult to reach firm conclusions on issues such as the distribution of synaptic current amplitudes at one release site or the degree of occupancy of postsynaptic receptors during synaptic activity (reviewed by 8, 15).

Several methods have been used to study synaptic transmission at single release sites. The simplest method is to select pairs of neurons that are connected together at a single synaptic terminal containing a single release site (29, 17, 1, 34). A release site, or active zone, is the morphological entity recognizable in electron micrographs, with a cluster of synaptic vesicles and, in excitatory synapses, a postsynaptic density. One synaptic terminal can therefore contain several release sites. The direct demonstration that a single release site is involved necessitates a study of serial electron micrographs of the stained pre- and postsynaptic neurons, a difficult procedure that has been followed in only one case so far (17). A second approach, which has been mainly applied in neuronal cultures, consists of applying locally a transmitter- releasing solution to a small volume of the postsynaptic dendritic field, ideally enclosing a single release site (4, 35, 23). Here, we present results obtained with a third approach, based on the stochastic activation of single release sites in brain slices by the potent vesicular release activator, α-latrotoxin.

α-Latrotoxin (α-LTX) is a neurotoxin purified from black widow spider venom, which triggers massive vesicular neurotransmitter release at active zones in vertebrate synapses (28, 7). The mode of action of the toxin is controversial. It has been proposed that α-LTX binds selectively to proteins interacting with the release machinery. In many cases, the resulting enhancement of transmitter release is Ca^{2+}-independent (26, 30, 6). It has also been shown that α-LTX forms cation-selective channels of high unitary conductance in lipid bilayers and in cell membranes (14, 18). These

channels are permeable to Ca^{2+} and are thought to increase transmitter release by elevating the intracellular Ca^{2+} concentration, thus accounting for the Ca^{2+}-dependent component of α-LTX-induced transmitter release that is observed in some preparations (3).

There are indications that the action of α-LTX can be highly localized. At the frog neuromuscular junction, α-LTX induces bursts of EPSPs at normal or elevated external Ca^{2+} concentrations, and these bursts were shown to arise at sharply localized regions of the nerve terminals by using extracellular mEPSC recording (10). In freeze fracture electron micrographs of frog neuromuscular junction nerve terminals exposed to α-LTX, some of the active zones display numerous marks of vesicle fusion, while other active zones from the same terminal remain as in control conditions (7). These results suggest that under certain conditions α-LTX could selectively activate single release sites.

The goal of the present work was to explore further the possibility that α-LTX can indeed activate individual release sites one at a time. For this study, we selected the inhibitory synapses formed among interneurons (basket and stellate cells) of the molecular layer of cerebellar slices. These cells have an electrically compact dendritic tree and a small input capacitance, thus allowing high quality recordings of synaptic currents (24). In this system, we found that α-LTX induces bursts of IPSCs that apparently originate at single release sites. From the study of the bursts, we have been able to calculate at single release sites the maximum postsynaptic receptor occupancy, the single channel conductance, the total number of channels, and the peak channel open probability. Furthermore, we demonstrate a large variability of the values of the last three parameters among individual release sites. Finally, we show that there are significant correlations between the values of certain parameters.

Results

α-Latrotoxin Induces Bursts of mIPSCs

Figure 1A illustrates mIPSCs collected in a cerebellar interneuron in the presence of tetrodotoxin (TTX). The amplitude distribution displayed a peak near 10 pA, the detection threshold of the analysis program, which was followed by a slowly decaying tail extending to several hundreds of pA. 24 presented similar data in this preparation and further demonstrated that the shape of the distribution histogram was not markedly modified by removing Ca^{2+} from the bath solution. These results indicate a large variability of mIPSC amplitudes in cerebellar interneurons. In the hope to gain insight into the mechanisms responsible for this variability, we investigated the effects of several agents known to increase vesicular release, including α-LTX. Bursts of IPSCs with homogeneous amplitudes were observed upon application of the toxin, suggesting that a small number of presynaptic release sites was activated during each burst. The dose of the toxin was reduced in subsequent experiments to reach a level where individual α-LTX-induced bursts would be clearly discernible.

All experiments began with a control period, during which spontaneous IPSCs were recorded in normal saline. TTX and NBQX, a blocker of AMPA-selective glutamate receptors, were then added to the bath. mIPSC frequencies varied among experiments from <1/min up to ~1 Hz (as in Figure 1A). Finally, α-LTX (0.1–1 nM) was applied for 2–5 min. No immediate change was observed, owing to the low dose and short exposure time that were used. The spontaneous synaptic activity

was then followed over a very long period of time (up to 90 min) in the continued presence of TTX and NBQX. Two delayed actions of the toxin could be distinguished. First, stepwise increases of the holding current, with unitary amplitudes near 20 pA, reflected the insertion of individual α-LTX channels in the membrane of the recorded cell (Figure 1B). These channels were occasionally observed to flicker between closed and open states before stabilizing in the open state (Figure 1C; in other examples, closed times of the channels were significantly longer than those illustrated.) In addition, each new channel insertion increased the noise of the current recording, presumably due to unresolved channel fluctuations. In practice, experiments had to be discontinued after the second or third toxin channel insertion to keep an acceptably low noise level. Fortunately, the rate of insertion of toxin channels was usually very low (1–5 insertions/hr). The second effect of the toxin was the appearance of bursts of mIPSCs (Figure 1D), resulting from an effect of the toxin on a presynaptic interneuron. These bursts also occurred at a very low rate. They could be immediately distinguished from single toxin channel currents, because events within bursts displayed the characteristic decay kinetics of control mIPSCs, as detailed below. However α-LTX-induced IPSCs differed from control mIPSCs in two important ways. First, the frequency of mIPSCs within bursts was much higher than that of control mIPSCs. Secondly, the amplitude distribution was much more homogeneous in α-LTX-induced bursts than in control conditions (compare Figure 1A with Figure 1D).

Simple and Complex α-LTX-Induced Bursts

Individual α-LTX-induced bursts were very variable. With 2 mM Ca^{2+} in the bath solution, burst durations ranged from 20 s to 2 min. Within a burst, the mean amplitude of mIPSCs was not always stable. Often a drop of mean amplitude was observed during the first seconds of a burst, as illustrated in Figure 2. In this case, the mean amplitude stabilized near 50 pA in the later part of the burst. Amplitude distributions for the entire burst and for a selected period where the mean amplitude seemed stationary could both be fitted with Gaussian curves (Figure 2B).

Figure 2C illustrates what appears as the superimposition of two bursts. In the first burst, the mean amplitude is initially 250 pA. It then drops to ~80 pA as the frequency of events progressively accelerates, and then slowly recovers its initial value as the frequency decreases again. Before the end of this recovery, however, a second burst starts with an initial amplitude near 60 pA, which then subsides to ~35 pA and remains stable over a period of >1 min.

The amplitude distribution histogram from the entire trace of Figure 2C has a complex shape (Figure 2D), and it superficially resembles the control mIPSC histogram of Figure 1A. However, when two regions from the trace corresponding to the steady state portions of each burst are selected, the amplitude distributions can be fitted with Gaussian curves (Figure 2D). The fit to the small amplitude burst gives a particularly low coefficient of variation value (CV = SD/mean; here, CV = 17%). This burst is further analyzed in Figure 3 and in Figure 5A below.

In other cases, still more complex bursts were observed, resulting from the superposition of simple bursts, where separation of underlying components was virtually impossible. These complex bursts were not analyzed further.

Estimate of Postsynaptic Receptor Occupancy

The finding of Gaussian amplitude distributions with specific means and low CV values suggests that each simple burst corresponds to the activation of a homogeneous population of receptors. The contrast between these narrow distributions and the broad distributions of control mIPSCs suggested that bursts originate at single release sites. As a further test of this possibility, we next

examined whether closely interspaced events within a burst interact with each other, following an approach previously used by 35 in hippocampal cultures. Figure 3A shows small portions of the small amplitude burst presented in Figure 2C. It is evident that the peak of IPSCs rising during the decay phase of the previous event and the peak of isolated IPSCs reach similar maximal values. We call A and A′ the amplitudes measured from the baseline to the peak and from the onset to the peak, respectively, of each IPSC. In Figure 3A, two events, labeled 1 and 2, are shown; the first event does not overlap with the preceding one, so that $A'_1 = A_1$, but it does overlap with its follower, so that $A'_2 < A_2$. Statistics were made over the entire burst of the dependence of A_2 and A'_2 on the interval from the previous event (δt). Whereas there was no marked dependence of A_2 on the interval for short values, A'_2 was found to decrease sharply at short δt values (Figure 3B and Figure 3C). The kinetics of this downward trend are comparable to the time course of decay of the average IPSC (Figure 3D). In addition, another process with a slower time constant is needed to describe the dependence of both A_2 and A'_2 on δt at intervals larger than 100 ms.

A simple explanation for the small onset-to-peak amplitudes at short δt values is that a high proportion of postsynaptic receptors is occupied at the peak of the mIPSC and that receptors become available again during the decline of the mIPSCs as deactivation proceeds. If the receptors were far from saturation at the peak of the synaptic currents, one would expect A'_2 to be independent of δt. The currents should summate linearly, and A_2 should tend to a 2-fold amplitude for very short intervals. On the other hand, if the postsynaptic receptors were fully saturated at the peak of the synaptic current, A_2 should be independent on the interval, and A'_2 should decrease toward 0 pA at short intervals, with kinetics that should match the decay of the average IPSC. The plots in Figure 3B and Figure 3C are close to this second pattern, indicating a high degree of receptor occupancy at the peak of the current.

The degree of receptor occupancy was more precisely estimated by extrapolating the fit of the A'_2 curve to δt = 0, as shown in Figure 3. The value found from the data of Figure 3C is 82%. The same analysis was carried out in a total of 14 bursts, giving occupancy values ranging from 56% to 114%, with a mean of 76% ± 16% (Table 1). The reliability of the extrapolation procedure was limited, mainly because each burst contained a comparatively small number of events at short δt values. This uncertainty accounts for the scatter in the results of individual bursts and for the occasional finding of occupancy percentages beyond 100%. As predicted, however, the mean value of the time constant of the occlusion, τ_{fast} (25.7 ± 2.4 ms), is almost the same as the weighted decay time constant τ_w (28.2 ± 3.1 ms), reflecting the overall decay kinetics of the IPSCs (see below).

Two alternative mechanisms could be invoked to explain the interaction observed between closely timed events: a presynaptic mechanism involving less transmitter release for the second event in a pair than for its predecessor, or desensitization of the postsynaptic receptors. The first mechanism would require that a vesicular release should drastically decrease the quantity of neurotransmitter liberated by the next exocytosis event; it is difficult to imagine a likely mechanism by which such an interaction could occur. In addition, it would be very unlikely if a presynaptic process followed the kinetics of the postsynaptic channels.

Concerning the second mechanism, desensitization of postsynaptic receptors, we first note that receptors must bind the agonist in order to desensitize, so that this mechanism would also imply a high receptor occupation. Second, according to current models of GABA receptor desensitization,

the receptors first accumulate in the desensitized state in response to a fast agonist pulse and exit this state in a second phase (19). Therefore, the population of desensitized receptors is expected to reach its peak later than the IPSC and to trail behind the IPSC decay during recovery. Only if the lifetime of the desensitized state was at least as short as that of the open state would the kinetics of the desensitized state parallel that of the open state. In such a case, the “desensitized” state, however, would not be distinguishable from the bound closed state leading to the open state. Altogether, the match between the kinetics of the occlusion and that of the mean IPSC implies that this occlusion cannot be ascribed to desensitization in the usual sense of the word.

Nevertheless, the fall of the mean amplitude during high frequency periods indicates that cumulative desensitization cannot be neglected. For the small amplitude burst shown in Figure 2C, this fall amounted to 1.5% per event. Because short intervals are more prevalent during the higher frequency parts of the burst, they tend to be associated with smaller amplitudes. The slow increase of A_2 and A'_2 with δt apparent in Figure 2B and Figure 2C therefore probably reflects cumulative desensitization.

In conclusion, the interaction observed between successive IPSCs is best explained by a high degree of receptor occupancy. This, together with the shape of the amplitude distribution within bursts, in turn implicates that the same population of receptors is exposed to neurotransmitter during following events. As it will be further discussed below, this means that a burst originates at a single release site.

Nonstationary Noise Analysis of Slow Bursts

Typical amplitude distributions of miniature synaptic currents in the CNS are very broad, presumably due to heterogeneity of miniature currents among different release sites and/or large variations in transmitter concentration. Nonstationary noise analysis (32) can give only very limited information on synaptic channels under these conditions. In view of the above results, suggesting that all events in a simple burst originate at one site, we next examined whether nonstationary variance analysis would give directly interpretable results in the present case. Because nonstationary noise analysis requires well separated events, it was necessary to reduce the frequency of events in α-LTX bursts. We found, in agreement with previous reports (e.g., 10), that the event frequency within bursts was dependent on the external Ca^{2+} concentration. By lowering the external Ca^{2+} concentration to 0.5 mM, bursts suitable for noise analysis were obtained (Figure 2C and Figure 4A). Figure 4 illustrates the principle of the analysis performed. A time window where we could easily differentiate the background synaptic activity was chosen for the analysis (Figure 4B, period between arrows). Events that were considered as coming from the background activity during the selected window are labeled in Figure 4B (4 events out of 95). These events fall outside of the Gaussian fit (Figure 4E) to the amplitude distribution of the events between arrows. Well separated events were then selected, such that the variance of adjacent events did not summate (Figure 4C). Figure 4D shows the calculated variance for the traces presented in C. The plot of the mean variance as a function of the mean current amplitude was well fitted with a parabola (Figure 4F). The parabolic fit can be used to calculate values for the elementary current, i_{el}, and for the number of channels underlying the IPSCs, N. In the present case, i_{el} = 2.1 pA and N = 102. The elementary conductance and the open probability of the channels at the peak of the synaptic currents were calculated from these results as γ = 34.8 pS and p_o = 0.35, respectively.

The fact that current-variance plots were parabolic and had initial slopes of the order expected for the unitary conductance of GABA-sensitive channels indicates that the main source of variance comes from single channel fluctuations.

Diversity Among the Noise Characteristics of Individual Bursts

Noise analysis results differed markedly among bursts (Table 2). Clear differences arose even when bursts were taken in the same postsynaptic cell. For example, the two bursts shown in Figure 5A and Figure 5B, which were obtained from the same neuron, yield different single conductance values (25.6 and 36.6 pS) and peak open channel probabilities (0.70 and 0.94).

The results of the ensemble noise analysis could be used to obtain an estimate of the CV of the amplitudes within a burst, after correction for the background noise. Corrected CV values varied between 3% and 25%, and had a mean of 13%. Because peak current amplitudes are correlated with the total number of channels, it was expected that the CV would show a negative correlation to mean current amplitude. In fact, however, no such correlation was found. Likewise, no correlation was apparent between p_o and γ. On the other hand, a highly significant negative correlation was found between p_o and N, showing that release sites with a large number of channels tend to have a small probability of opening (Figure 5C).

Overall, we conclude that the values found for three important functional parameters differ among individual bursts. Differences in N and γ among bursts imply that individual release sites are associated with aggregates of postsynaptic GABA-sensitive channels that differ in number and unitary conductance.

Variability among the Decay Kinetics of Individual Bursts

Inspection of superimposed IPSCs coming from different bursts suggested that the kinetics of mIPSC decay were distinct for each burst. For example, the burst shown in the upper panel of Figure 6A contains only slowly decaying currents, whereas the burst of the lower panel, which was taken from the same interneuron, contains only fast decaying currents. Scaled averages from these two bursts are shown in Figure 6B. In order to compare results from all bursts, which were fitted either to single or to double exponential functions, a weighted time constant was defined as $\tau_w = \tau_1 \times W_1 + \tau_2 \times W_2$, where W_1 and W_2 are proportional to the amplitudes of the fast and slow components, respectively. The monoexponential decay of Figure 6B has a τ_w value 3.46 times larger than the biphasic decay superimposed to it. τ_w varied from 10 to >60 ms and was significantly correlated to p_o values, such that slow decays were associated to high p_o (Figure 6C).

These results show that each release site possesses its own decay kinetics, and that even bursts located on the same postsynaptic cell can be very distinct from this point of view.

Discussion

Simple Bursts Occur at Single Release Sites

The homogeneity of IPSC amplitudes and kinetics within bursts and the evidence for current occlusion imply that all events within such a simple α-LTX-induced burst lead to the activation of the same subset of postsynaptic receptors. Theoretical considerations and experimental evidence

gathered at AMPA-selective glutamatergic synapses indicate that a substantial occupancy of postsynaptic receptors is achieved only at the site where glutamate is released, and that cross-activation of neighboring sites is significant only for simultaneous release at shortly interspaced sites, as occurs, for instance, at calyceal synapses (8, 2). While cross-activation may occur at NMDA-sensitive glutamatergic synapses due to the high affinity of the corresponding receptors for their agonist, it is unlikely to take place at GABAergic synapses, since the parameters that affect intersite cross-talk (number of transmitter molecules per vesicle, diffusion constant of the transmitter, affinity of the receptors) are, to the best of our knowledge, similar for GABAergic and for AMPA-selective glutamatergic synapses (8). The functional unit defined by an α-LTX-induced burst is therefore attributed, in the following discussion, to a single release site. However, in the absence of precise electron microscopy data, the possibility of a few neighboring sites acting as a single functional release site cannot be ruled out.

Mechanism of Action of α-LTX

The frequency of mIPSCs during bursts is Ca^{2+}-dependent in our preparation. A similar effect has been previously found at the frog neuromuscular junction (10, 13), as well as after treatment with high concentrations of the toxin (3–300 nM) in hippocampal organotypic slices (6). Moreover, the rates of occurrence of bursts and of α-LTX-induced single channel currents were comparable. Since α-LTX channels are permeable to Ca^{2+}, bursts may reflect a local elevation of Ca^{2+} concentration in the presynaptic neuron following the opening of an α-LTX channel. How local the Ca^{2+} concentration change needs to be is a matter of speculation. Comparison of the mean amplitudes of IPSCs before and after addition of TTX suggests that interneuron–interneuron synapses involve one or a few release sites (24). Thus, even a rather widespread Ca^{2+} elevation in the presynaptic terminal may lead to the activation of a single release site.

Amplitude Distributions

In a burst, the amplitude distribution of mIPSCs was fitted by a single Gaussian curve, as it is at the neuromuscular junction. In the central nervous system, the amplitude distributions of miniature synaptic currents is typically skewed toward large events (11; see also Figure 1A). One possible interpretation of this finding is that the sizes of miniature currents originating in various release sites are heterogeneous (11). However, another possibility is that the distribution of amplitude sizes at single sites is skewed. The only data available at inhibitory synapses is a study by 16 in cultured amacrine cells. These cells form synapses with two postsynaptic receptor clusters (“dinapses”). Broad and skewed amplitude distributions were found at dinapses, and they were interpreted as resulting from variations in neurotransmitter concentration. Two studies using local application of sucrose or of divalent cations on excitatory synapses in hippocampal cultured neurons also indicated a very broad and skewed amplitude distribution at single release sites (4, 23). However, a third study, using a similar methodology, concluded to very variable widths of amplitude distributions, and occasionally single Gaussian distributions with CV values as low as 6% could be observed (35). Amplitude histograms of evoked EPSPs/EPSCs recorded from single site synapses in interneurons of hippocampal slices and in cerebellar granule cells yielded Gaussian distributions with CV values near 25% (17, 1, 33). On the whole, the distribution of mIPSCs at the interneuron–interneuron synapse is more symmetrical and narrower than in most of these earlier results.

Variability of Mean Amplitudes between Sites

A 14-fold variability of the mean amplitude was observed from burst to burst (Table 1 and Table 2), implying a high variability between sites. This is a very wide range, but it does not cover the full range observed for mIPSCs from a single postsynaptic cell, and the mean amplitudes in the bursts were, on average, smaller than the mean value of mIPSC histograms. Part of the discrepancy comes from the fact that the values in Table 1 and Table 2 were calculated from the stable part of the bursts, sometimes after the amplitude had decreased. In addition, our analysis apparently selected sites with small mIPSC amplitudes; we occasionally recorded bursts of high amplitude, but they were usually associated with bursts originating at other sites so that we could not perform the analysis, except for the burst presented in Figure 2C. 23 observed a 4-fold range in mean site amplitude between cells, but in their study median values of mEPSC amplitudes were homogeneous for a single postsynaptic cell. In contrast to their findings, we measured clear differences in unit sizes for bursts recorded in the same interneuron.

Receptor Occupancy at the Peak of mIPSCs

Two independent sets of measurements indicated a high maximum occupancy of postsynaptic receptors. First, consecutive mIPSCs were shown to reach a similar peak amplitude even when they occurred during the decay phase of the previous mIPSC, so that the onset-to-peak amplitude decreases sharply with the interval from the last event (δt). We estimated the postsynaptic receptor occupancy at the peak of the IPSCs by extrapolating this relationship to $\delta t = 0$. The mean occupancy found in this way was 76%.

The second piece of evidence for high occupancy came from noise analysis. According to current models for receptor activation, the receptor occupancy is larger than, or equal to, the peak open channel probability p_o (33). Since noise analysis yielded large p_o values (>0.8) for some of the bursts, the receptor occupancy must have been very large at least in these bursts.

The effects of benzodiazepines on IPSC amplitudes have also been used to assess receptor saturation at GABAergic synapses. The results indicated a high degree of saturation for acute and organotypic slice preparations (9, 27) but a low occupancy in cultured amacrine cells (16). Quantal analysis at GABAergic synapses in brain slice preparations indicated equally spaced quantal peaks with nonincreasing variance (12, 31). Altogether, it seems that there is a high degree of occupation of postsynaptic GABA receptors in slice preparations, but that the situation may be different in cultured neurons.

Low Degree of Desensitization of Interneuron GABA Receptors

Contrary to a recent study in hippocampal culture (19), we conclude that in cerebellar interneurons a single IPSC leads to a minimal amount of desensitization. The discrepancy may come from differences between the receptors involved. IPSCs have a faster time course in interneurons than that observed in hippocampal cells. The interaction observed between events in interneurons resembles the data obtained in hippocampal neurons with the low affinity agonist β-alanine. It is thus possible that a low GABA affinity is responsible for the faster decay kinetics and low level of fast desensitization in interneurons. Alternatively, the transition to the fast desensitization state (D_{fast}) hypothesized by Jones and Westbrook may be slower in cerebellar interneurons than in hippocampal neurons. In this case, less channels will enter the desensitized state, and more will

open. Therefore, p_o is expected to be higher than in the model of Jones and Westbrook (0.6–0.8). Consistent with this expectation, p_o values above 0.9 were observed in some bursts.

Variability of Elementary Synaptic Characteristics

The parameters characterizing mIPSCs (p_o, i_{el}, N, and τ_w) strongly differ among bursts. Interestingly, differences in p_o, N, and τ_w were found even for bursts obtained from the same postsynaptic neuron, showing that the identity of the postsynaptic neuron cannot be the exclusive factor underlying intersite variability. One obvious possible interpretation of the results is that the properties of postsynaptic receptors located at each synaptic site are specific. This could happen either because of the presence of specific subunits of GABA receptors or because of modulation of receptors by local signaling (e.g., phosphorylation by protein kinases). In favor of the first possibility 21 found that individual synaptic boutons at retinal synapses are associated with specific subsets of GABA receptors and, furthermore, that boutons synapsing on the same postsynaptic neuron correspond to different receptors sets. Even though a postsynaptic component to the variability is likely, the possibility cannot be ruled out that presynaptic factors or the geometry of the synaptic contact contribute to the observed differences. 24 reported a main conductance state of 28 pS in the interneurons, very close to the mean value derived from nonstationary noise analysis (27 pS; Table 2). But the single channel conductance varied between bursts from 12.7–41.5 pS. This variability is unlikely to result from dendritic filtering, because at this time in development (14–16 days old), interneurons exhibit rather short (<50 μm) and thick (>1 μm) dendrites (C. Pouzat and S. Kondo, personal communication), and because the unitary conductance was neither correlated with the mIPSCs rise time ($\gamma < 27$ pS: 1.37 ± 0.4 ms; $\gamma > 27$ pS: 1.16 ± 0.25 ms) nor with the series resistance of the recordings ($\gamma < 27$ pS: R_s = 23.6 ± 13.2 MΩ; $\gamma > 27$pS: R_s = 33.1 ± 20.9 MΩ). In other preparations, many conductance states have been reported (reviewed by20). Using in situ hybridization 22 revealed in cerebellar interneurons α_1, β_2, and γ_2 subunits, as well as small amounts of the α_3 subunit. Future work will be required to reconcile the small number of subunit combinations suggested by these data with the very variable γ values apparent in Table 2.

A negative correlation was found between p_o and N. Assuming that receptor clusters have a fixed density, large values of N would be associated with large postsynaptic clusters. In such a scheme, vesicular release near the cluster center would lead to a larger average dilution for bursts with high N values than for bursts with small N values.

Values of τ_w, the weighted time constant used to assess the slowness of IPSC decay, varied across single sites over a 6-fold range. At inhibitory synapses onto cerebellar granule cells, IPSCs become faster with development, presumably as a result of the gradual expression of the α_6 subunit (5, 36). There is no detectable expression of α_6 subunits at any developmental stage in the molecular layer, but IPSCs in interneurons also become faster with development (C. Pouzat, personal communication). The speed of IPSC decay may, therefore, reflect the proportion of mature receptors contained in one specific cluster. The positive correlation between p_o and τ_w would then suggest that mature channels have both a faster closing rate and a lower maximal probability of opening than juvenile ones.

Implications for Quantal Analysis in the Central Nervous System

The present findings have implications regarding the interpretation of amplitude distributions of evoked IPSCs. A skewed single site amplitude distribution would blur the quantal peaks in evoked currents distribution; whereas, with a Gaussian distribution, peaks should emerge. Due to high receptor occupancy, the release of several vesicles at a single release site does not generate equally spaced peaks in amplitude distributions of evoked IPSCs, but rather a single peak. Multiple peaks would result from the summation of IPSCs from several release sites and would be equally spaced only if the quantal size was identical at all sites.

Experimental Procedures

Slice Preparation

Cerebellar slices were prepared as described earlier (25). Briefly, young rats (14–16 days old) were killed by decapitation under anesthesia with Metofane, the cerebellum was removed, and slices (180 μm in thickness) were cut in the vermis, parallel to the sagittal plane. Slices were kept in a vessel bubbled with 95% O_2 and 5% CO_2 at 33°C for 1–6 hr before being used for recordings.

Patch-Clamp Recordings

Patch-clamp recordings were made from inhibitory interneurons (stellate and basket cells) in the molecular layer of the cerebellum. These cells can be readily differentiated from migrating granule cells by the size of their soma (~8 μm in diameter), their spiking behavior observed in cell-attached mode, and the presence of IPSCs and EPSCs in the whole-cell recording mode. The tight-seal whole-cell recording technique was used for all experiments. When filled with internal saline, recording pipettes had a resistance of 3–5 MΩ. For the analysis of postsynaptic receptor occupancy, experiments were performed with K^+-containing internal solutions containing 150 mM KCl, 4.6 mM $MgCl_2$, 0.1 mM $CaCl_2$, 1 mM K EGTA, 10 mM K HEPES, 0.4 mM NaGTP, and 4 mM NaATP; or 120 mM KCl, 4.6 mM $MgCl_2$, 1 mM $CaCl_2$, 10 mM K EGTA, 10 mM K HEPES, 0.4 mM NaGTP, and 4 mM NaATP. For nonstationary noise analysis, a Cs^+-containing internal solution of the following composition was used: 124 mM CsCl, 4.6 mM $MgCl_2$, 1 mM $CaCl_2$, 10 mM BAPTA, 10 mM HEPES, 0.4 mM NaGTP, and 4 mM NaATP. Membrane currents were recorded at a holding potential of −60mV. The mean cell capacitance and uncompensated series resistance values were 4.5 ± 1.1 pF and 25.6 ± 15.5 MΩ, respectively. The series resistance was compensated between 60% and 80%. During experiments, the preparation was visualized through a 63× water immersion objective.

The bath was continuously perfused at a rate of 1–1.5 ml/min with a physiological saline containing 125 mM NaCl, 2.5 mM KCl, 1 mM $MgCl_2$, 1.25 mM NaH_2PO_4, 26 mM $NaHCO_3$, and 10 mM glucose. For the first set of experiments, this medium was supplemented with 2 mM $CaCl_2$. This was also the external solution used for preparing and keeping the slices prior to recording. Two of the experiments analyzed for noise analysis were recorded with this external Ca^{2+} concentration; for all of the others, 0.5 mM $CaCl_2$ was used. The external solution was continuously bubbled with a

mixture of 95% O_2 and 5% CO_2 to maintain the pH at 7.4. All experiments were performed at room temperature.

Chemicals

Tetrodotoxin (TTX, 200 nM; Sigma Chemical Company, Saint Louis, MO) and the glutamate receptor antagonist 6-nitro-7-sulphamoylbenzo[f]quinoxaline-2,3-dione (NBQX, 10 μM; Tocris Neuramin Limited, Bristol, UK) were applied to the recording chamber prior to toxin application and were maintained throughout the experiment. α-LTX was purchased from Latoxan, Rosans, France. We used two batches of the toxin, which had different effective activities, and which were used at concentrations of 0.1 and 1 nM, respectively. The toxin was bath-applied for 2–5 min in the presence of 0.1% bovine serum albumin (Sigma).

Data Acquisition and Analysis

Since the frequency of α-LTX-induced bursts was very low, it was not practical to acquire the entire length of the experiment on a computer. Data were therefore acquired first on tape. Bursts of mIPSCs were localized in time and subsequently reacquired, either at 250 μs per point after filtering at 0.8 kHz or at 100 μs per point after filtering at 1 kHz. mIPSCs were analyzed using a software written by C. Pouzat, which used a detection threshold with a typical value of 10 pA. For the events which exceeded threshold, the onset-to-peak amplitude, the absolute amplitude of the peak, the time at the peak, and the time to 50% of the peak were stored. The baseline current of the recording just before the burst was subsequently subtracted from the absolute peak amplitude to obtain the baseline-to-peak amplitude. The interval from the previous mIPSC (δt) was calculated as the time at the peak of the event minus the time at the peak of the previous event. Those parameters were used for the analysis of the occupancy of postsynaptic receptors and for that of the amplitude distribution of mIPSCs. When measuring onset-to-peak amplitudes of closely interspaced events, a correction was made to account for the decay occurring in the first IPSC while the second rose to its peak. An average time course A(t) was calculated from well isolated events in the burst. In a pair, the percentage of current decrease of the first event during the rise time of the second is calculated as $P = [A(\delta t) - A(\delta t + r)]/ A(\delta t)$, where δt is the interval to the second event and r is the rise time of the A(t) curve. P was used to correct the onset-to-peak amplitude measurement, A'_2, according to $A'_{2, corr} = A'_2 + P (A_2 - A'_2)$, where $A'_{2, corr}$ is the corrected value of A'_2.

Bursts were defined as a sequence of more than 20 events that had a frequency exceeding by at least 5-fold that of background events. The latter frequency was measured during the minute preceding the burst, except in one case where this was not possible due to overlap with a preceding burst. On this basis, 44 bursts were selected. Each burst contained up to 400 events. Out of the 44 bursts, 10 were multiple bursts that could not be decomposed into simple bursts, 10 were rejected because they contained excessive background activity, and the remaining 24 bursts gave the results summarized in Table 1 and Table 2 .

Nonstationary Noise Analysis

The mIPSCs were selected to perform nonstationary noise analysis (32) as follows. Detected mIPSCs were aligned with respect to the time to half maximum amplitude. Sweeps containing artifacts were rejected. Well isolated events were then selected, to avoid an artifactual variance

contribution from adjacent events. Usually, the burst was separated from the background synaptic activity on amplitude criteria, as illustrated in Figure 4. If the burst exhibited a clearly distinctive time course of decay, a selection based on the time course of the events was sometimes performed in place of the amplitude selection. The selected events were then grouped into subgroups of successive 5–10 events. This allowed us to minimize variance contributions due to slow variations in amplitude or in baseline current (32). The average current and variance over time were calculated for each subgroup as $y_m(t) = 1/S \times \Sigma\, y_i(t)$ and $var(t) = 1/(S - 1) \times \Sigma\, [y_i(t) - y_m(t)]^2$ where $y_i(t)$ is the current signal at time t for trace number i, $y_m(t)$ is the average current at time t, and S is the number of sweeps per group. The mean (I) and variance (V) were subsequently averaged for all the subgroups, and the background variance was subtracted. The plot of variance versus mean current was fitted using a least square minimization procedure with a parabola of the form $V(I) = i_{el}I - I^2/N$.

The parameters i_{el} and N were recovered from the fit. The amplitude of the average current at the peak (I_{peak}) was measured, and p_o was calculated as $p_o = I_{peak}/Ni_{el}$.

The single channel conductance underlying the events is $\gamma = i_{el}/(V_h - E_{Cl})$ where V_h is the holding potential, and E_{Cl} is the reversal potential for chloride (0 mV). The coefficient of variation of the analyzed events was calculated as $CV = [V(I_{peak}) - V(0)]^{1/2}/I_{peak}$. It is this CV estimate which is entered in Table 2.

For the purpose of display, variance-amplitude plots were binned. Time intervals were first chosen such that the average IPSC decreased with regular amplitude decrements at each interval (usually 5 pA). Amplitudes and variances were averaged for each subgroup over these time intervals. Amplitude and variance were finally averaged among subgroups and corresponding SEM values were computed.

Acknowledgements

We thank Christophe Pouzat for writing the detection software and for helpful discussions. This work was supported by the Deutsche Forschungsgemeinschaft (SFB 406) and by a fellowship from the French Ministère de la Recherche et de la Technologie to C. A.

References

1 Arancio, O., Korn, H., Gulyàs, A., Freund, T., and Miles, R. (1994). Excitatory synaptic connections onto rat hippocampal inhibitory cells may involve a single transmitter release site. J. Physiol. *481*, 395–405.

2 Barbour, B., and Häusser,M. (1997). Intersynaptic diffusion of transmitter. Trends Neurosci., in press.

3 Barnett, D.W., Liu, J., and Misler, S. (1996). Single-cell measurements of quantal secretion induced by alpha-latrotoxin from rat adrenal chromaffin cells: dependence onextracellular Ca2*1*.Pflügers Arch. *432*, 1039–1046.

4 Bekkers, J.M., Richerson, G.B., and Stevens, C.F. (1990). Origin of variability in quantal size in cultured hippocampal neurons and hippocampal slices. Proc. Natl. Acad. Sci. USA *87*, 5359–5362.

5 Brickley, S.G., Cull-Candy, S.G., and Farrant, M. (1996). Development of a tonic form of synaptic inhibition in the rat cerebellar granule cells resulting from persistent activation of GABAA receptors. J. Physiol. *497*, 753–759.

6 Capogna, M., Gähwiler, B.H., and Thompson, S.M. (1996). Calcium independent actions of *a*-latrotoxin on spontaneous and evoked synaptic transmission in the hippocampus. J. Neurophysiol. *76*, 3149–3158.

7 Ceccarelli, B., Grohovaz, F., and Hurlbut, W.P. (1979). Freeze-fracture studies of frog neuromuscular junctions during intense release of neurotransmitter. I. Effects of black widow spider venom and Ca2+-free solutions on the structure of the active zone. J. Cell Biol. *81*, 163–177.

8 Clements, J.D. (1996). Transmitter timecourse in the synaptic cleft: its role in central synaptic function. Trends Neurosci. *19*, 163–171.

9 De Koninck, Y., and Mody, I. (1994). Noise analysis of miniature IPSCs in adult rat brain slices: properties and modulation of synaptic GABAA receptor channels. J. Neurophysiol. *71*, 1318–1335.

10 del Castillo, J., and Pumplin, D.W. (1975). Discrete and discontinuous action of brown widow spider venom on the presynaptic nerve terminals of frog muscle. J. Physiol. *252*, 491–508.

11 Edwards, F.A. (1995). Anatomy and electrophysiology of fast central synapses lead to a structural model for long-term potentiation. Phys- Rev. *75*, 759–787.

12 Edwards, F.A., Konnerth, A., and Sakmann, B. (1990). Quantal analysis of inhibitory synaptic transmission in the dentate gyrus of rat hippocampal slices: a patch-clamp study. J. Physiol. *430*, 213–249.

13 Fesce, R., Segal, J.R., Ceccarelli, B., and Hurlbut, W.P. (1986). Effects of black widow spider venom and Ca2+ on quantal secretion at the frog neuromuscular junction. J. Gen. Physiol. *88*, 59–81.

14 Finkelstein, A., Rubin, L.L., and Tzeng, M.C. (1976). Black widow spider venom: effect of purified toxin on lipid bilayer membranes. Science *193*, 1009–1011.

15 Frerking, M., and Wilson, M. (1996). Saturation of postsynaptic receptors at central synapses? Curr. Opin. Neurobiol. *6*, 395–403.

16 Frerking, M., Borges, S., and Wilson, M. (1995). Variation in GABA mini amplitude is the consequence of variation in transmitter concentration. Neuron *15*, 885–895.

17 Gulyàs, A.I., Miles, R., Sìk, A., Tòth, K., Tamamaki, N., and Freund, T.F. (1993). Hippocampal pyramidal cells excite inhibitory neurons through a single release site. Nature *366*, 683–687.

18 Hurlbut, W.P., Chieregatti, E., Valtorta, F., and Haimann, C. (1994). Alpha-latrotoxin channels in neuroblastoma cells. J. Membr. Biol. *138*, 91–102.

19 Jones, M.V., and Westbrook, G.L. (1995). Desensitized states prolong GABAA channel responses to brief agonist pulses. Neuron *15*, 181–191.

20 Kaila, K. (1994). Ionic basis of GABAA receptor channel function in the nervous system. Prog. Neurobiol. *42*, 489–537.

21 Koulen, P., Sassoe-Pognetto, M., Grunert, U., and Wässle, H. (1996). Selective clustering of GABA(A) and glycine receptors in the mammalian retina. J. Neurosci. *16*, 2127–2140.

22 Laurie, D.J., Seeburg, P.H., and Wisden, W. (1992). The distribution of 13 GABAA receptor subunit mRNAs in the rat brain. II. Olfactory bulb and cerebellum. J. Neurosci. *12*, 1063–1076.

23 Liu, G., and Tsien, R.W. (1995). Properties of synaptic transmission at single hippocampal synaptic boutons. Nature *375*, 404–408.

24 Llano, I., and Gerschenfeld, H.M. (1993). Inhibitory synaptic currents in stellate cells of rat cerebellar slices. J. Physiol. *468*, 177–200.

25 Llano, I., Marty, A., Armstrong, C.M., and Konnerth, A. (1991). Synaptic- and agonist-induced excitatory currents of Purkinje cells in rat cerebellar slices. J. Physiol. *434*, 183–213.

26 Longenecker, H.E., Jr., Hurlbut, W.P., Mauro, A., and Clark, A.W. (1970). Effects of black widow spider venom on the frog neuromuscular junction. Effects on end-plate potential, miniature end-plate potential and nerve terminal spike. Nature *225*, 701–703.

27 Poncer, J.-C., Dürr, R., Gähwiler, B.H., and Thompson, S.M. (1996). Modulation of synaptic GABAA receptor function by benzodiazepines in area CA3 of rat hippocampal slice cultures. Neuropharmacology *35*, 1169–1179.

28 Pumplin, D.W., and Reese, T.S. (1977). Action of brown widow spider venom and botulinum toxin on the frog neuromuscular junction examined with the freeze-fracture technique. J. Physiol. *273*, 443–457.

29 Raastad, M., Storm, J.F., and Andersen, P. (1992). Putative single quantum and single fiber excitatory postsynaptic currents show similar amplitude range and variability in rat hippocampal slices. Eur. J. Neurosci. *4*, 113–117.

30 Rosenthal, L., and Meldolesi, J. (1989). Alpha-latrotoxin and related toxins. Pharmacol. Ther. *42*, 115–134.

31 Schneggenburger, R., and Konnerth, A. (1992). GABA-mediated synaptic transmission in neuroendocrine cells: a patch-clamp study in a pituitary slice preparation. Pflu¨ gers Arch. *421*, 364–373.

32 Sigworth, F.J. (1980). The variance of sodium current fluctuations at the node of Ranvier. J. Physiol. *307*, 97–129.

33 Silver, R.A., Cull-Candy, S.G., and Takahashi, T. (1996). Non-NMDA glutamate receptor occupancy and open probability at a rat cerebellar synapse with single and multiple release sites. J. Physiol. *494*, 231–250.

34 Stevens, C.F., and Wang, Y. (1995). Facilitation and depression at single central synapses. Neuron *14*, 795–802.

35 Tang, C.M., Margulis, M., Shi, Q.Y., and Fielding, A. (1994). Saturation of postsynaptic glutamate receptors after quantal release of transmitter. Neuron *13*, 1385–1393.

36 Tia, S., Wang, J.F., Kotchabhakdi, N., and Vicini, S. (1996). Developmental changes of inhibitory synaptic currents in cerebellar granule neurons: role of GABA(A) receptor alpha 6 subunit. J. Neurosci. *16*, 3630–640.

Table 1 Summary of the Analysis of Postsynaptic Receptor Occupancy

	Burst Number															
	1	2	3	4	5	6	7	8	9	10	11	12	13	14	Mean	SD
I_{peak} (pA)	195.5	93.4	42.3	37.9	38.5	79.0	55.7	82.4	45.5	79.9	35.5	65.6	99.4	25.0	69.7	43.2
% Occupancy	57	81	68	91	82	56	79	58	75	69	67	98	80	114	76.0	15.8
τ_{fast}(ms)	12.7	33.9	21.8	41.6	13.7	26.2	22.1	20.6	35.5	34.0	26.0	23.4	13.7	17.6	25.7	8.56

I_{peak} is the average peak amplitude, % occupancy is the percentage of postsynaptic receptors occupied at the peak of the synaptic current, and τ_{fast} is the fast time constant of the biexponential fit to the plot of the onset-to-peak amplitude versus interval (Figure 3C).

Table 2 Summary of the Parameters Estimated by Nonstationary Noise Analysis

	Burst Number															
	11	12	13	14	15	16	17	18	19	20	21	22	23	24	Mean	SD
I_{peak} (pA)	38.6	65	74	25.6	20.3	19.5	14	37	25.0	18.3	60.1	39.0	28.3	77.0	38.7	21.6
CV (%)	13.4	9.3	14.2	13.2	16.8	3.4	13.8	11.6	9.4	13.4	17.5	10.4	25.3	16.7	13.5	5.0
γ (pS)	17.7	30.0	34.8	12.7	26.9	25.2	17.0	25.6	27.5	36.6	41.5	19.5	28.4	37.9	27.1	8.7
p_o	0.45	0.60	0.35	0.47	0.41	1	0.68	0.70	0.88	0.94	0.24	0.59	low	low	0.54	0.28
N	81	61	102	71	31	12	20	34	17	9	100	57	ND	ND	49.6	33.8
τ_w (ms)	13.5	29.5	32.8	20.4	9.8	64.0	31.4	27.5	41.4	46.4	20.9	24.2	27.8	22.7	29.4	13.9

Bursts 11–14 are also presented in Table 1. I_{peak} is the average peak amplitude, CV is the coefficient of variation of the peak amplitude, γ is the single channel conductance, p_o is the channel peak open probability, N is the number of postsynaptic channels, and τ_w is the weighted time constant describing the IPSCs decay. For the last 2 bursts, p_o was too low to obtain a proper fit of the variance-versus-mean relationship, so it is simply noted as 'low', and N was not determined (ND).

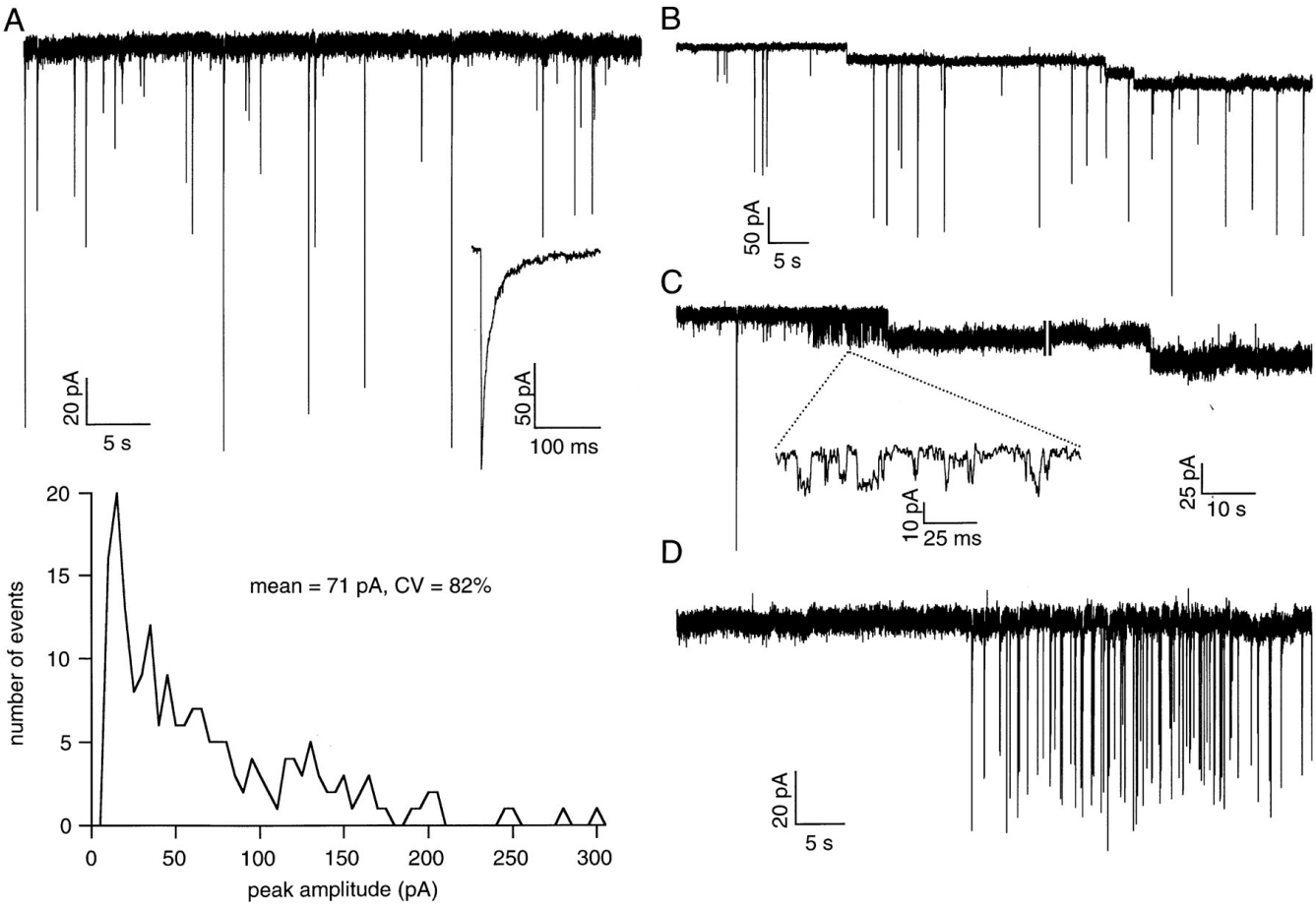

Figure 1Control and α-Latrotoxin-Induced mIPSCs in Interneurons

(A) Characteristics of control mIPSCs recorded in an interneuron in the presence of 200 nM TTX and 10 μM NBQX. Upper trace: mIPSCs are infrequent and have widely different amplitudes. Lower trace: amplitude distribution recorded in a period of 12 min (193 mIPSCs). The distribution is highly skewed toward large values and has a high CV (82%).

(B) Following a transient application of α-LTX at 0.5 nM, several stepwise increases in the baseline current are observed, corresponding to the irreversible opening of α-LTX channels. Some superimposed mIPSCs can be observed. The baseline noise increases following each opening.

(C) Another example of α-LTX-induced single channel currents. One channel fluctuates between open and closed states before reaching a permanently open state. Fluctuations are shown at a higher time scale in the inset.

(D) Burst of mIPSCs 13 min after the application of 0.1 nM of α-LTX. Within a burst, mIPSCs have much more homogeneous amplitudes than control mIPSCs. Records in (A), (B), (C), and (D) are from different interneurons.

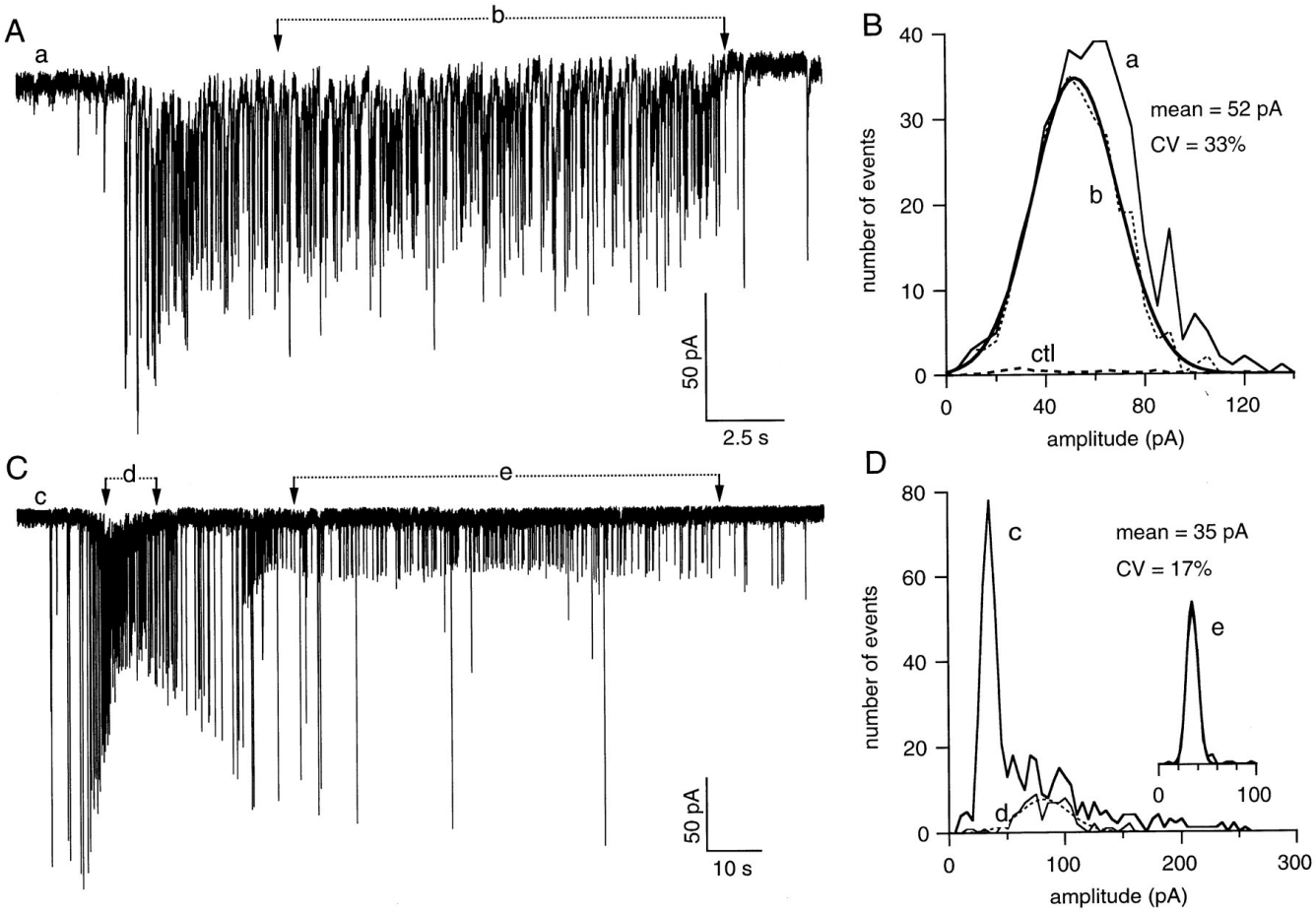

Figure 2 The Amplitude Distribution of mIPSCs during a Burst Is Gaussian

(A) Burst of mIPSCs induced by α-LTX in the presence of 2 mM external Ca^{2+}. Both the beginning and the end of the burst are well defined. The frequency of events is about 12 Hz for 19 s. The mean amplitude decreases during the first few seconds of the burst and stabilizes subsequently.

(B) Distributions of the mIPSCs amplitude measured from baseline to peak for the entire burst in A (a) and for the period between arrows (b). The thin line (a) has a Gaussian shape with a mean near 60 pA. The dotted line (b) is fitted to a Gaussian (thick line) with a mean of 52 pA and a CV of 33%. The amplitude histogram obtained before addition of the toxin is shown (control, dashed line).

(C) Example of a complex α-LTX-induced burst. The external Ca^{2+} concentration was 0.5 mM. Two bursts of mIPSCs of distinct amplitude can be distinguished. The first one starts at the beginning of the trace and is composed of mIPSCs of high amplitude. The amplitude decreases soon after the start of the burst as the frequency increases. Then the frequency goes down again, and the amplitude progressively returns to its initial value. A second burst of smaller amplitude starts toward the end of the first. Initially, its amplitude decreases and then stabilizes when the frequency has declined. Labels: (c) denotes the whole trace, (d) and (e) denote the periods when the amplitude of the first and second bursts, respectively, are more stable.

(D) Amplitude distributions measured from baseline to peak during the periods (c), (d), and (e) (inset). Gaussian fits have been superimposed on (d) (dotted line) and (e). Distribution (e) is almost indistinguishable from the corresponding fit. Mean and CV were calculated from the parameters of the Gaussian fit of (e). Note that mean amplitudes differ among the 3 bursts, and that the distributions (b), (d), and (e) all have a Gaussian shape with a CV value much lower than that of the control distribution of Figure 1A.

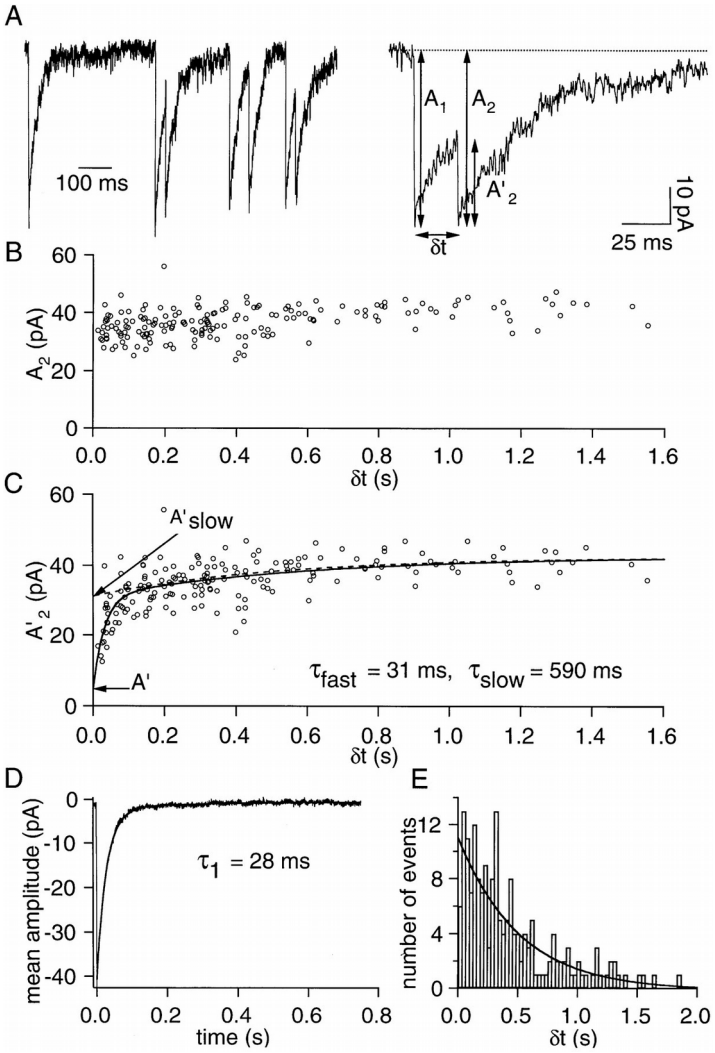

Figure 3 Determination of the Occupancy of Postsynaptic Receptors during an α-LTX-Induced Burst

(A) Left and right traces are portions of the small amplitude burst shown in Figure 2C at a more expanded time scale. The parameters measured for the analysis are defined on the right trace. A_1 and A_2 are the amplitudes of two successive IPSCs measured from baseline to peak, A'_2 is the amplitude of the second event measured from onset to peak, and δt is the interval from the previous IPSC. The analysis is performed on the stable portion of the second burst (e) in Figure 2C.

(B) A_2 increases slightly with δt, but there are no strong variations for short δt values.

(C) A'_2 increases sharply with δt at short intervals (up to 100 ms) and then increases more slowly to the end of the investigated intervals. The plot is fitted with a double exponential, with time constants τ_{fast} = 31 ms, τ_{slow} = 590 ms, and with corresponding weights of 69% and 31%.

(D) Average IPSC calculated from 33 events within the burst. The peak of the average has been aligned to t = 0 so that time scales are identical in (B), (C), and (D). The average is well fitted by a monoexponential with a time constant of 28 ms, close to τ_{fast} in panel C. Plots (B) through (D) together indicate a high degree of postsynaptic receptor occupancy. The calculation of the occupancy assumes that A'_2/A_1 is the fraction of receptors that are free from neurotransmitter. To obtain a mean value of A_1 which is corrected for the overall reduction of IPSC amplitudes at higher frequencies, the slow component of the A'_2 (δt) curve was extrapolated to δt = 0 (A'_{slow}). The mean value of the free receptors corresponds to the intersect of the biexponential fit with the ordinates (A

′). The peak occupancy was therefore calculated as $(A'_{slow} - A')/A'_{slow}$, giving here 82%. Implicit in the calculation is the assumption that channels occur in only two states, a doubly occupied state that is unamenable to activation ($A'_{slow} - A'$) and an unoccupied state that can be activated by the neurotransmitter (A′). Consistent with this assumption, the fraction of monoliganded channels during the decay time of an IPSC predicted from the kinetic model of Jones and Westbrook (1995) is negligible compared to that of doubly liganded channels.
(E) The distribution of δt is well fitted by a single exponential (τ = 0.51 s), indicating that the release triggered by α-LTX is a Poisson process.

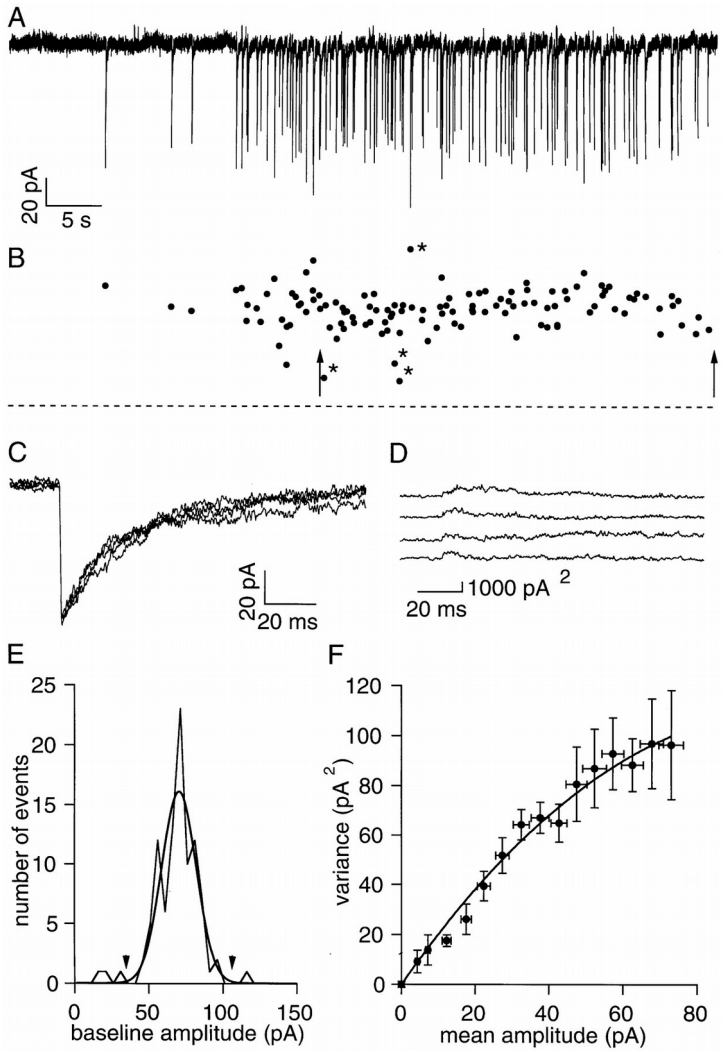

Figure 4 Nonstationary Noise Analysis of Slow Bursts

(A) A slow burst of mIPSCs obtained in 0.5 mM external Ca^{2+} concentration after exposure to α-LTX.

(B) A plot of the baseline-to-peak IPSC amplitudes as a function of time. The arrows indicate the region selected to perform nonstationary noise analysis. It is chosen as a period during which the background synaptic activity is easily isolated from the events belonging to the burst. (At the beginning of the burst, a period of higher variability is apparent. This is most likely due to contamination with background synaptic activity.) Between arrows, four events (labeled *) are considered as belonging to the background activity.

(C) Examples of consecutive traces selected for noise analysis. They have been aligned on the time to half peak amplitude.

(D) Variance of the traces in (C) around the mean.

(E) Baseline-to-peak amplitude distribution for the period between arrows in (B). The events attributed to background activity in (B) stand out of a Gaussian fit to the distribution of all events (arrowheads).

(F) Plot of the mean variance versus the mean amplitude. The baseline variance (7.5 pA^2) was subtracted. Two parameters are recovered from the fit: the number of channels underlying the events, N, and the elementary current, i_{el}. In this case, N = 102 channels and i_{el} = 2.1 pA. The open channel probability calculated at the peak of the synaptic current is p_o = 0.35.

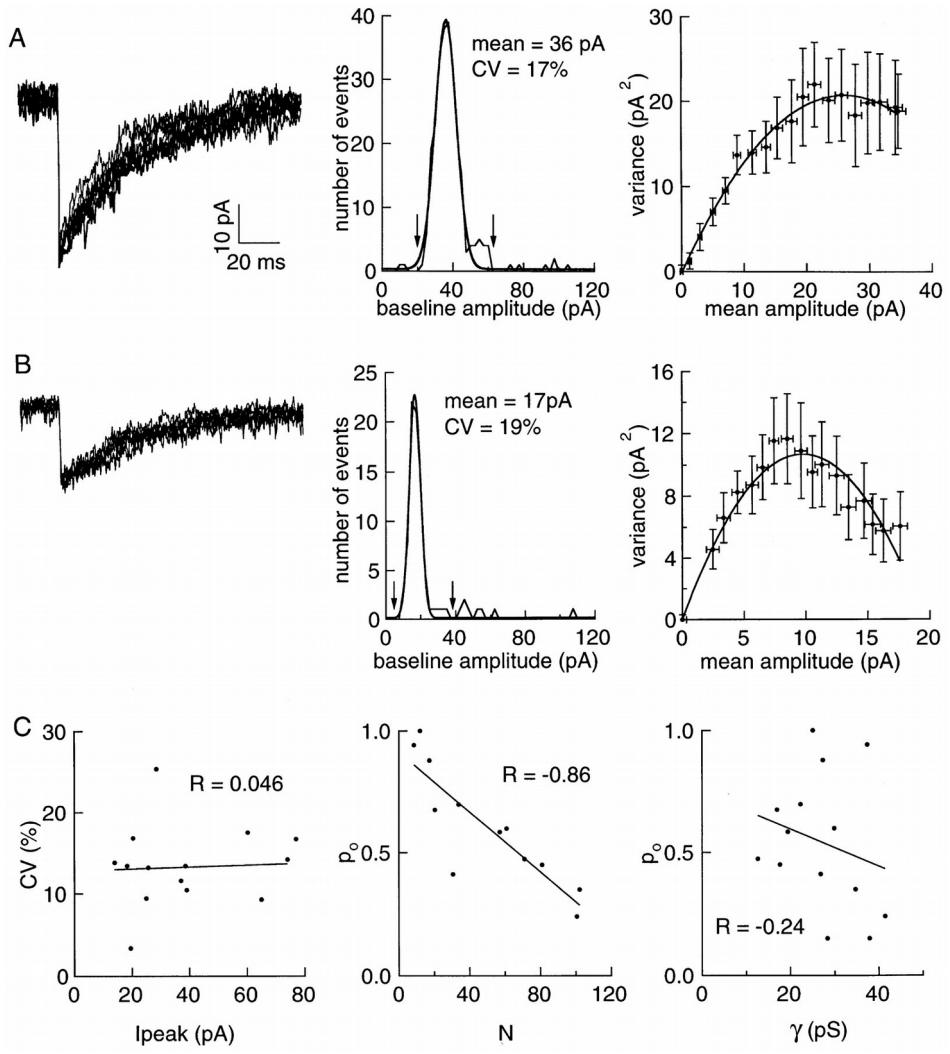

Figure 5 Elementary Synaptic Parameters Vary among Different Release Sites

(A) Left: 9 consecutive traces selected for nonstationary noise analysis, from the small amplitude burst shown in Figure 2C. Center: baseline-to-peak amplitude distribution of the whole burst with a superimposed Gaussian fit. The excess of events between 50 and 65 pA correspond to the larger amplitude events during the initial high frequency period. Mean and CV calculated from the parameters estimated by the fit are indicated. Right: plot of the variance (10 × 10 subgroups) versus mean amplitude. The baseline variance (4.6 pA^2) was subtracted. The plot is fitted to a parabola, yielding i_{el} = 1.54 pA, N = 34 channels, γ = 25.6 pS, and p_o = 0.70.

(B) Analysis from another burst, obtained in the same cell as in (A). Left, 6 consecutive traces selected for nonstationary noise analysis. Center, baseline-to-peak amplitude distribution of the whole burst fitted with a Gaussian. Right, variance versus mean amplitude plot (10 × 7 subgroups). Baseline variance (3.3 pA^2) was subtracted; i_{el} = 2.2 pA, N = 9, γ = 36.6 pS and p_o = 0.94.

(C) Correlation plots between three pairs of synaptic parameters obtained from nonstationary noise analysis, from data gathered in 14 different bursts. There is no correlation between CV and mean peak amplitude (left), or between p_o and single channel conductance (right), but there is a significant negative correlation between p_o and N (center; Spearman rank order test, $p < 0.001$). Regression coefficients (R) are indicated.

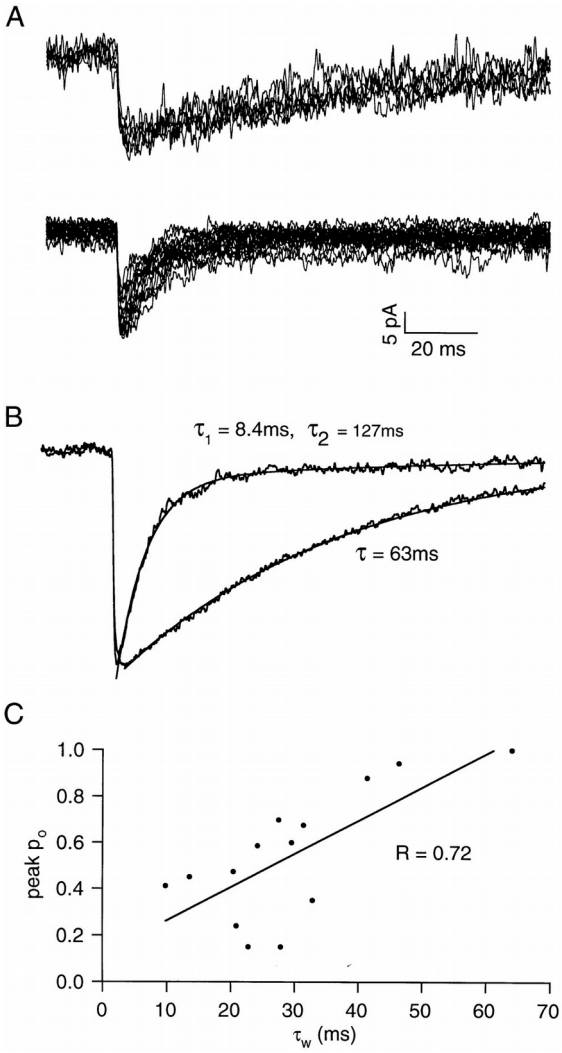

Figure 6 Kinetics Variability between Release Sites

(A) Two sets of time-aligned mIPSCs selected for the nonstationary noise analysis coming from two distinct bursts recorded in the same cell. While the peak amplitude of the bursts are similar, the decay kinetics of the events are very different.

(B) Normalized mean current kinetics for the two bursts in (A). One decay is fitted with a monexponential having a time constant of 63 ms. The other decay is fitted using a biexponential curve with time constants τ_1 = 8.4 ms and τ_2 = 127 ms and with corresponding weights W_1 = 92% and W_2 = 8%.

(C) Plot of peak p_o versus $\tau_w = \tau_1 \times W_1 + \tau_2 \times W_2$. The value of τ_w reflects the overall slowness of the decay of the mean IPSC. There is a significant correlation between peak p_o and τ_w (Spearman rank order test, $p < 0.02$).